



ELSEVIER

Available online at www.sciencedirect.com

SCIENCE @ DIRECT®

Nuclear Instruments and Methods in Physics Research A ■ (■■■■) ■■■–■■■

**NUCLEAR
INSTRUMENTS
& METHODS
IN PHYSICS
RESEARCH**
Section A

www.elsevier.com/locate/nima

Quenching effects in nitrogen gas scintillation

Hideki Morii^a, Kentaro Mizouchi^a, Tadashi Nomura^{a,*}, Noboru Sasao^a,
Toshi Sumida^a, Makoto Kobayashi^b, Yoshiyuki Murayama^{c,1},
Ryuichi Takashima^c

^a Department of Physics, Kyoto University, Kyoto 606-8502, Japan^b High Energy Accelerator Research Organization (KEK), Ibaraki 305-0801, Japan^c Department of Physics, Kyoto University of Education, Kyoto 612-8522, Japan

Received 12 September 2003; received in revised form 21 January 2004; accepted 10 February 2004

Abstract

We report on the studies of quenching effects in N₂ scintillation. Our main interest is to find a practical gas that reduces the scintillation yield in air substantially. We have studied O₂, CO₂, and CH₄ in N₂, and have determined their Stern–Volmer constant. When two quenching gases are used in a mixture, the effects are found to be additive. The quenching mechanism of these gases is discussed and its practical application is reported.

© 2004 Elsevier B.V. All rights reserved.

PACS: 29.40.Mc

Keywords: Gas scintillation; Quenching; KOPIO

1. Introduction

Nitrogen gas scintillation has been known to exist for a long time, and has been employed as a particle detector in many experiments [1–6]. It is an essential phenomenon for these detectors, but is rather harmful for some applications. This is exactly the case for a detector we are now preparing.

This detector, called a beam catcher, is a part of a bigger detector system in an experiment named

KOPIO [7]. The experiment itself is to measure the branching ratio of $K_L \rightarrow \pi^0 \nu \bar{\nu}$ with a single event sensitivity of $\sim 6 \times 10^{-13}$. The beam catcher is placed inside a K_L beam, and its role is to distinguish high-energy gamma rays (100–1000 MeV) coming from K_L decays from the much more abundant neutrons. The beam catcher itself will be detailed elsewhere. Below we briefly describe it to clarify our motivation for the study reported here. The beam catcher is composed of many identical modules; each module is essentially a sandwich calorimeter consisting of a lead plate, an aerogel tile, light collecting mirrors, and a photomultiplier tube (PMT). We note that there is an air gap between the aerogel and the mirror. The PMT detects the Cherenkov light produced in the

*Corresponding author.

E-mail address: nomurat@scphys.kyoto-u.ac.jp

(T. Nomura).

¹ Present address; FSIABC Inc, Kanagawa 247-0072, Japan.

aerogel radiator by the electrons and positrons of an electromagnetic shower. It is essential for the experiment to reduce as much as possible the misidentification probability, i.e. the probability of detecting neutrons as gamma rays. This is the very reason we must employ a Cherenkov radiator with a low refractive index, instead of the more commonly used scintillator; it is relatively insensitive to heavy charged particles.

As stated, there is an air gap between the radiator and the light collecting mirror, and this would give background counts due to nitrogen scintillation. This scintillation yield can be completely neglected as far as the high-energy gamma ray detection is concerned. Namely, the expected number of photoelectrons due to the N_2 scintillation is much smaller than that from Cherenkov photons created by the gamma rays of our interest. However, neutrons, which are by far the most abundant particles passing through the catcher module, would produce charged particles which in turn make scintillation light in the air. The background signal observed in the PMT is expected to be single-photon random pulses; the PMT would behave as if it had an additional dark current source. Thus, we made a GEANT3 [8] simulation to calculate this noise current, and concluded that in the worst case it would result in unsatisfactory PMT operation, such as high trigger rate and/or gain change, etc.² It is, thus, desirable to reduce this background scintillation; actually, we set our goal to reduce it by a factor of 3–4, considering that it would then be dominated by other intrinsic noise sources produced by neutron reactions. We note that it is impractical to install the aerogel and/or mirrors in a vacuum vessel. Thus, the only way is to find a quenching gas to suppress the nitrogen scintillation.

The paper is organized as follows. Section 2 describes our experimental setup, data taking, and analysis procedures. In Section 3, the results are presented with discussions. Section 4 is devoted to the conclusions.

²The ambiguity in the conclusion was due to uncertainties in the neutron spectrum and their interactions used in the simulation.

2. Experiment

2.1. Setup

To compare the scintillation yields in various gases, we evaluate the light yield per energy deposit in the gas. In this experiment, scintillation lights, registered by α -particles of known energy, are detected by two photomultipliers. Energy deposit in the gas is evaluated by measuring α -particles' final energies after they traverse the gas. In order to avoid uncertainty due to geometrical effects, the measurements are performed with various flight distances of α -particles.

The experimental setup is shown in Fig. 1. It consists of a gas-tight vessel made with crossed SUS404 pipes, two 2-in. PMTs to view scintillation light through the top and bottom quartz windows, an α -ray source attached to the head of a rod, a PIN photodiode (PD) to measure the kinetic energy of α -particles, and a light emitting diode (LED) used to check and monitor the PMTs. The actual α -source is ^{241}Am ; it emits 5.486-MeV (85%) and 5.443-MeV (13%) α -particles. The photodiode is a Hamamatsu [9] S3590-09 [10], which has no protection layer on the injection surface. It is used to create a trigger signal upon detection of α -particles, and to measure their remaining kinetic energy after passing through the gas. The distance between the source and photodiode (denoted by L_{sp}) can be varied by

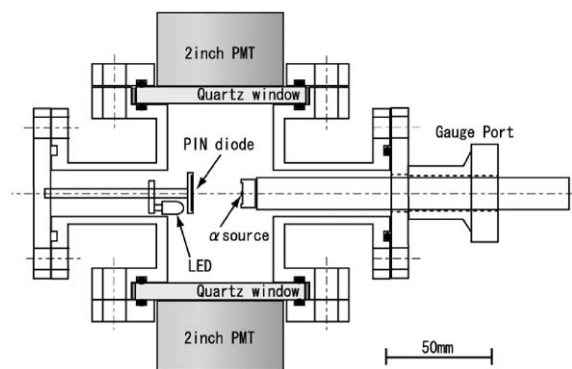


Fig. 1. Cross-sectional view of experimental setup. α -particles emitted from ^{241}Am source lose their energy in gas and are caught by PIN diode (PD). Scintillation light is detected with two PMTs on the top and bottom of the vessel.

pushing or pulling the rod. The PMTs in use are Hamamatsu R2256-02 and R329-02 [11]; they have a bialkali cathode with quartz (R2256-02) or borosilicate glass (R329-02) window, respectively. Pure and mixed gases are introduced into the vessel after evacuating it for at least 5 min. The mixing ratio is controlled by adjusting flow rate, and is monitored by gas flow meters. We estimate uncertainty in the gas mixing rate to be about 5%. All measurements are done at one atmospheric pressure, and a room temperature of 22°C.

2.2. Data acquisition system and data taking procedure

Fig. 2 shows a schematic diagram of our readout system. The PD signal is first amplified by a pre-amplifier, and then discriminated. The threshold level is set to 1.0 MeV. Its output is fed into two gate generators, which provide the gates to two types of analog-to-digital converters (ADC); one is a pulse-height sensitive ADC for the PD signal (1- μ s-long gate), and the other is a charge sensitive ADC for the PMTs (80-ns-long gate). With a trigger signal, a data taking cycle is initiated by a computer, and all ADC data are read via a CAMAC system.

We prepare five kinds of gases; nitrogen (N_2), dry air, oxygen (O_2), carbon dioxide (CO_2), and methane (CH_4). The mixing ratio is changed by a step of about 10%. For each gas mixture, the source–photodiode distance (L_{sp}) is varied from 5 to 30 mm by a step of 5 mm. Each data point consists of about 40,000 triggers.

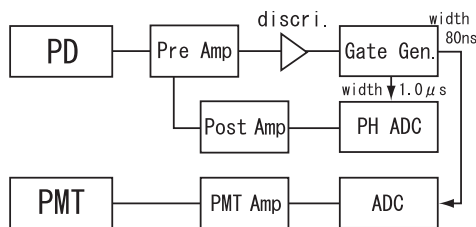


Fig. 2. Readout system in schematic diagram. Circuit is triggered by PD signal with a threshold level of 1.0 MeV in α -particle kinetic energy. With trigger, gate generators make two gates with different widths (80 ns and 1 μ s), and the ADC of PMT and PD are read.

2.3. Data analysis procedure

In this subsection, we present our data analysis procedure, taking the data of pure nitrogen gas as an example. Fig. 3 shows an example of the PD pulse height distribution; this particular data is taken at $L_{sp} = 15$ mm. Fig. 4 shows corresponding ADC spectra for the PMTs. First of all, we fit a Gaussian function to the PD spectrum, and require events to be within $\pm 2\sigma$ around the peak.

The two vertical lines in Fig. 3 indicate the cut boundaries. The lower (upper) curves in Fig. 4 are the PMT spectrum after (before) this cut. We then calculate the number of photoelectrons (n_{pe}) from this spectrum, for which we employ two different methods: one is to calculate inefficiency (the sharp peak on the left in Fig. 4), and the other is to calculate the mean of the spectrum. In both cases, we assume the Poisson statistics to hold for the observed photoelectrons. In the former method, the inefficiency is expressed by

$$P_0 = \exp(-\langle n_{pe} \rangle) \quad (1)$$

where P_0 represents the probability of observing no photoelectron (i.e. inefficiency), and $\langle n_{pe} \rangle$ is the average number of photoelectrons. In reality,

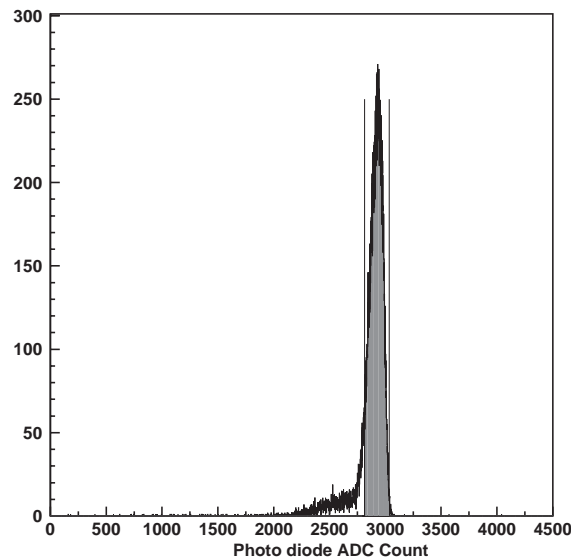


Fig. 3. Typical PD spectrum taken at $L_{sp} = 15$ mm in pure N_2 , corresponding to 4.2 MeV in α -particle kinetic energy. Shaded area shows the $\pm 2\sigma$ region around the peak.

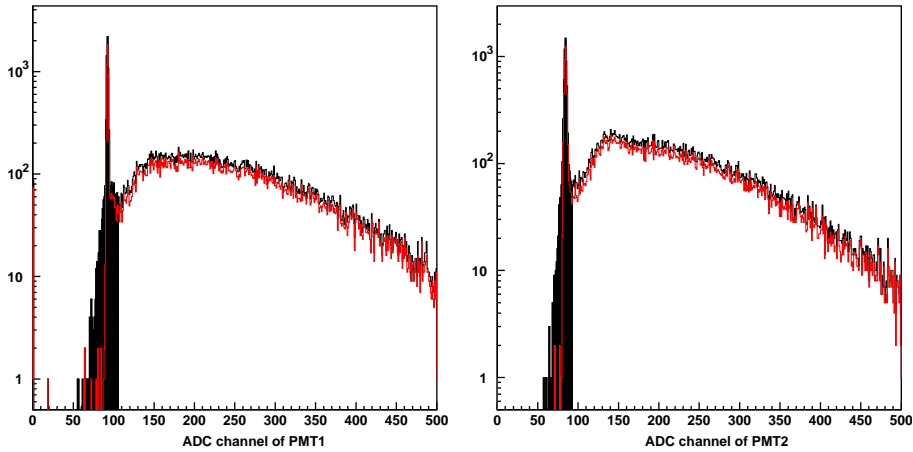


Fig. 4. Typical PMT spectrum taken at $L_{sp} = 15$ mm in pure N_2 for PMT1 (left) and PMT2 (right). The lower (upper) curves are the PMT spectrum after (before) PD spectrum cut and shaded region shows the inefficiency counts.

Table 1

Number of photoelectrons obtained with two methods for pure N_2 at $L_{sp} = 15$ mm

Method	PMT1 (R2256-02)	PMT2 (R329-02)
Inefficiency	2.01 ± 0.07	1.95 ± 0.08
Single photoelectron	1.98 ± 0.04	1.95 ± 0.04

we define the inefficiency as the counts below the lowest point between the zero and single photoelectron peaks. For example, the shaded region in Fig. 4 shows the inefficiency counts.

In the latter method, we calculate the mean of the spectrum, and divide it by the one photoelectron peak channel, which is obtained by a separate calibration run with the LED. The number of photoelectrons obtained with these methods are listed in Table 1.

Two points are of our interest in the table. First of all, since PMT1 has sensitivity in a wider wavelength region, it may observe in principle larger number of photoelectrons. In reality, the results from PMT1 and PMT2 are in good agreement, indicating the N_2 scintillation is predominantly in the visible region, where both PMT1 and PMT2 have identical sensitivities. We will discuss this in more detail in Section 3.1. The second point to be noted is agreement in the two measurement methods. The measurements at other distances and/or with other gas mixtures indicate

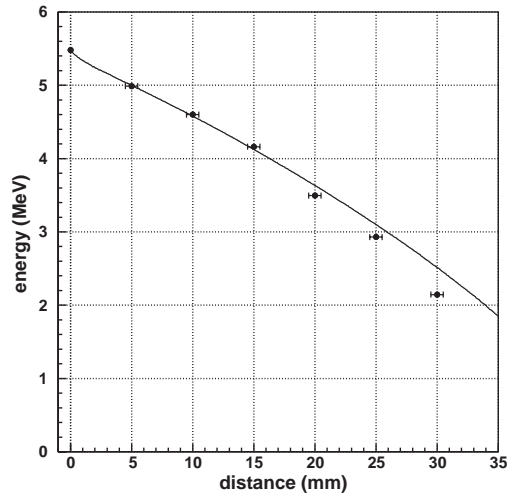


Fig. 5. PD peak as function of L_{sp} for pure N_2 . The horizontal error bars represent the uncertainty of α -source position. The vertical errors are negligibly small. The solid curve is the result of GEANT3 simulations.

they always yield consistent results. In the following, we quote only the results from the inefficiency method because the other method (single photoelectron) is found somewhat vulnerable to PMT gain change.

The next step in the analysis procedure is to deduce energy loss ΔE of α -particles in the gas. Fig. 5 shows the peak of the PD spectrum (such as

shown in Fig. 3) as function of L_{sp} . In this plot, the peak position at zero distance is assigned to 5.48 MeV. The solid curve is the result of GEANT3 simulations. As seen, they agree fairly well with each other, although a small discrepancy exists at large L_{sp} . We regard that the PD signal (measured value) represents the kinetic energy remained after the dE/dx loss in the gas. For example, at the distance of $L_{sp} = 15$ mm, the α -particle loses the energy of $\Delta E = 5.48 - 4.20 = 1.28$ MeV in the gas.

Fig. 6 shows the number of photoelectrons per unit energy loss, $n_{pe}/\Delta E$, as function of L_{sp} . Also shown is a geometrical acceptance calculated with a simulation code. The vertical errors assigned to the data points represent the statistical errors, and the horizontal error shows an uncertainty (± 0.5 mm) assigned to the location of the α -source (positioning error). The vertical errors assigned to the geometrical acceptance are the difference in acceptance when the source has the positioning error quoted above.

In order to calculate the total number of photons emitted by the gas per unit energy loss (dN_{ph}/dE), we need to know the quantum efficiency of the PMT photocathode and also the emission spectrum of the N_2 scintillation. For the sake of simplicity, we completely neglect the

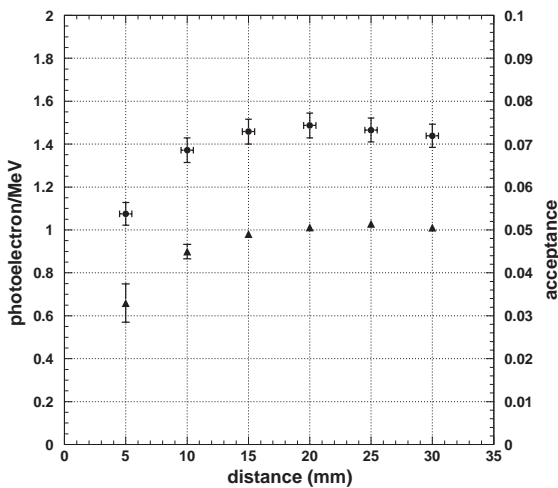


Fig. 6. Number of photoelectrons per 1 MeV energy loss (solid dots with crossing error bars) for pure N_2 . The geometrical acceptance is shown by the triangle points.

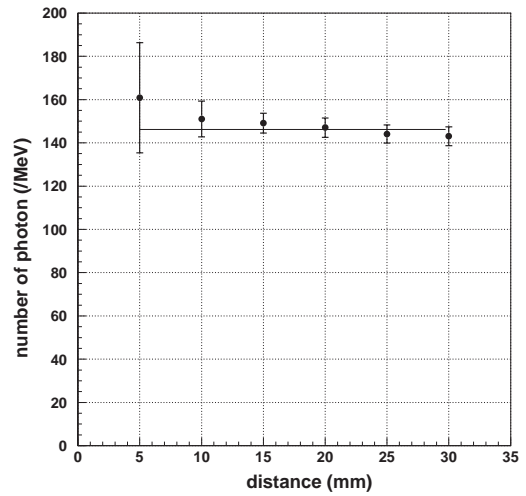


Fig. 7. dN_{ph}/dE as function of L_{sp} for pure N_2 . The vertical errors represent statistical errors combined with the effect of α -source positioning uncertainty.

emission in the UV region (see Table 1), and assume a flat spectrum in the visible region. Averaging over the quantum efficiency curve provided by Hamamatsu [12], we find the average value to be 20%. We estimate that this value has an error of $\sim 10\%$.³ In the following, all the values quoted as dN_{ph}/dE should be understood to have this scale error.

Fig. 7 shows the plot of dN_{ph}/dE versus L_{sp} . The errors come from statistics and those in the geometrical acceptance, which in turn stem from the α -source positioning uncertainty. They are combined in quadrature.

As expected, the measured points are independent of the distance L_{sp} .⁴ We define the value $\langle dN_{ph}/dE \rangle$ to be the best fit of these values; this

³The estimate is largely based upon our past experience; the quantum efficiency depends upon tube-to-tube characteristics and/or tube's age. In our case, PMT1 may have a lower value than PMT2; this is inferred from the disagreement between our observation of no UV-emission and the data reported by Duquesne and Kaplan [13], who reported the 20% N_2 scintillation in the UV region. Incompatibility depends upon assumed emission spectrum in UV; however, 10% scale error in the average quantum efficiency seems to be adequate.

⁴These particular data seem to have some systematic tendency by accident. However, the same kind of data for other gas mixtures do not have such tendency.

is indicated by the horizontal line in Fig. 7. For the pure nitrogen, we find

$$\begin{aligned} \langle dN_{\text{ph}}/dE \rangle &= 141.1 \pm 2.1 \quad (\text{PMT1}) \\ &= 146.2 \pm 2.1 \quad (\text{PMT2}). \end{aligned}$$

These values are consistent with the value given by Birks [14].

3. Results and discussions

3.1. Scintillation light yield for pure gases and air

In this subsection, we present our results for 4 pure gases (N_2 , O_2 , CO_2 , and CH_4) and dry air. In order to calculate photon yield, we need to know the emission spectrum for each gas at least in the visible region. Since we are unable to find it, below we simply use the same average quantum efficiency of 20% as that of N_2 . Table 2 lists the values of $\langle dN_{\text{ph}}/dE \rangle$ for 4 pure gases and dry air.

As can be seen from Table 2, there is no big difference between PMT1 and PMT2 for all gases, justifying the assumption that the emission is predominantly in the visible region. Hereafter, we only quote the results from PMT2, considering that we will actually use this type of photocathode and window material.

3.2. Quenching effect in pure nitrogen

In this subsection we show the results of quenching effect in pure N_2 . When quencher gas (oxygen, for example) is mixed into pure nitrogen, energy transfer such as $\text{N}_2^* + \text{O}_2 \rightarrow \text{N}_2 + \text{O}_2^*$ occurs and O_2^* decays non-radiatively. Here, N_2^* and O_2^*

symbolically represent any excited states created by ionization or collision. This mechanism, called quenching, reduces the light yield of scintillation. If the fraction of the quencher gas is small, quenching effect is represented by a model by Stern and Volmer [15], expressed by

$$N_{\text{ph}} = \frac{N_{\text{ph}}^0(N_2)}{1 + Kc} \quad (2)$$

where $N_{\text{ph}}^0(N_2)$ represents the light yield from pure nitrogen, K the Stern–Volmer constant and c the fraction of the quenching gas. The constant K measures the importance of the quenching effect. In our experimental conditions, Eq. (2) is expected to hold for $c \ll 1$.

A phenomenological model can be developed to extend the applicability of original Stern–Volmer equation to the full range of c . The derivation of the model can be found in Appendix A, together with a brief description of the original model. The modified model is expressed as

$$\begin{aligned} N_{\text{ph}} &= \frac{1}{1 + Kc} (1 - c)N_{\text{ph}}^0(N_2) + cN_{\text{ph}}^0(Q) \\ &\quad + c(1 - c)N_{\text{ph}}(Q \rightarrow N_2) \end{aligned} \quad (3)$$

where $N_{\text{ph}}^0(Q)$ is the light yield of a pure quencher gas and $N_{\text{ph}}^0(Q \rightarrow N_2)$ measures the effect of energy transfer from quencher gas to radiative excited states of N_2 . Fig. 8 shows the measurement results obtained for the $\text{N}_2\text{--O}_2$ gas mixture.

The ordinate represents $\langle dN_{\text{ph}}/dE \rangle$ while the abscissa is the fraction of oxygen gas. The solid curve shows a fit with Eq. (3). In this fit, we assume $N_{\text{ph}}^0(N_2)$ and $N_{\text{ph}}^0(Q)$ are given by the data at $c = 0$ and 1, respectively. (See the values of PMT2 in Table 2 for $N_{\text{ph}}^0(N_2)$ or $N_{\text{ph}}^0(Q)$ actually used.) We find K and $N_{\text{ph}}(Q \rightarrow N_2)$, free parameters in the fit, are $K = 20.7 \pm 1.5$ and $N_{\text{ph}}(Q \rightarrow N_2) = 7.1 \pm 2.1$, respectively. The dashed curve in Fig. 8 is a fit with the original Stern–Volmer model (Eq. (2)). Here the fit region is restricted to $c = 0\text{--}0.4$. We note that although Eq. (2) is only valid for $c \ll 1$, it reproduces the data points well up to $c \sim 0.4$. This is because the effects of $(1 - c)$ in the 1st term and $c(1 - c)N_{\text{ph}}^0(Q \rightarrow N_2)$ in the 3rd term tend to cancel each other. The resultant Stern–Volmer constant from this fit is $K = 26.4 \pm 1.5$. Birks [14] quotes $K = 20$ from Grun and Schopper [16]; since this

Table 2

The number of scintillation photons per 1 MeV energy loss ($\langle dN_{\text{ph}}/dE \rangle$)

Gas	PMT1 (R2256-02)	PMT2 (R329-02)
N_2	141.1 ± 2.1	146.2 ± 2.1
Air	25.46 ± 0.43	26.06 ± 0.46
O_2	0.61 ± 0.22	0.46 ± 0.22
CO_2	5.09 ± 0.28	4.90 ± 0.27
CH_4	1.39 ± 0.09	1.32 ± 0.08

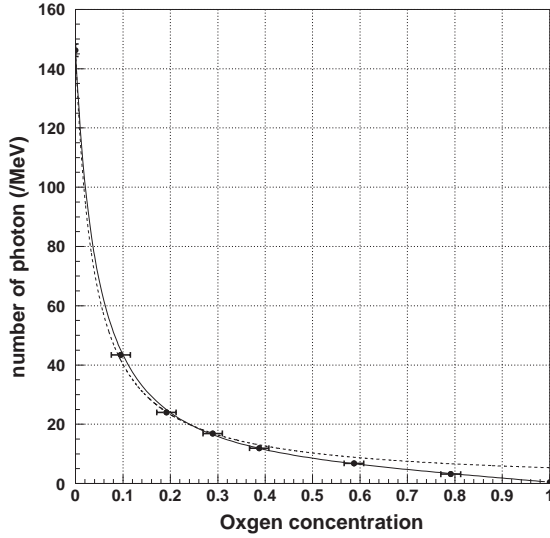


Fig. 8. O₂ quenching effect in N₂. The solid and dashed curves show the fits with modified ($c = 0-1$) and original ($c = 0-0.4$) Stern–Volmer models, respectively. The fitting region is shown in the parentheses.

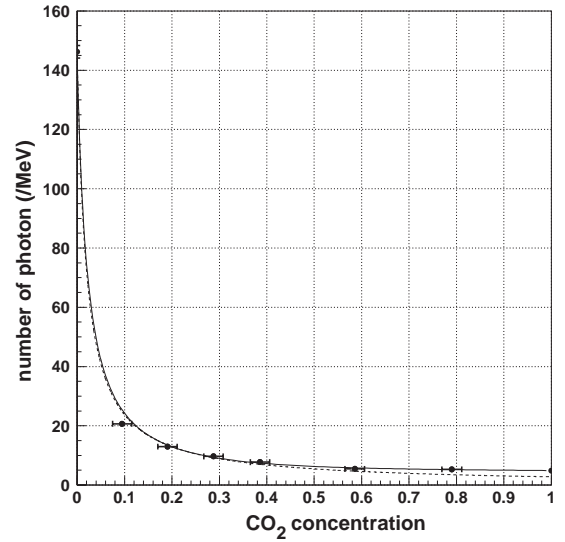


Fig. 9. CO₂ quenching effect in N₂. The solid and dashed curves show the fits with modified ($c = 0-1$) and original ($c = 0-0.4$) Stern–Volmer models, respectively. The fitting region is shown in the parentheses.

experiment was done at a pressure of 585 mmHg, the value corresponds to $K = 25$ at our conditions. We conclude that this value agrees with both of our results although it is slightly closer to one obtained with Eq. (2).

Fig. 9 (Fig. 10) shows the same plot for the mixture of N₂ and CO₂ (N₂ and CH₄), together with the curves obtained by a similar procedure. In all cases, the modified Stern–Volmer model (Eq. (3)) reproduces the data points very well in the full range of c . We summarize the results in Table 3, in which χ^2/ν represents the chi-square per degree of freedom in the fit.⁵

3.3. Quenching effect in air

In this subsection, we present the results of quenching effect in the case that the quencher gas is mixed in air. For the mixture of three gases, the quenching effect is expected to work additively.

⁵The values of χ^2 are all small compared with their expected value of ν . This fact indicates possible overestimate of errors assigned to the data points. However, we leave them as they are because the fits seem satisfactory, judging from Figs. 8–10.

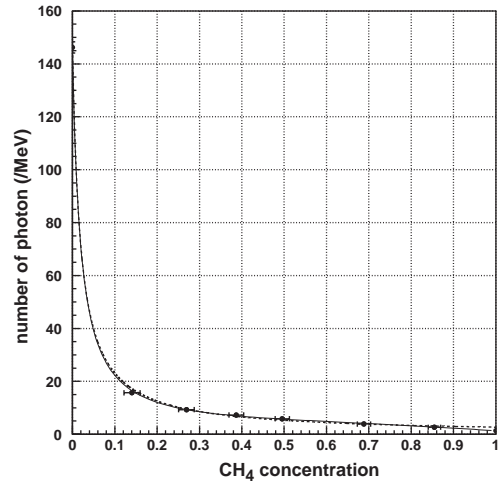


Fig. 10. CH₄ quenching effect in N₂. The solid and dashed curves show the fits with modified ($c = 0-1$) and original ($c = 0-0.4$) Stern–Volmer models, respectively. The fitting region is shown in the parentheses.

Thus, Eq. (3) can be modified to

$$N_{\text{ph}} = \frac{(1 - c_1 - c_2)}{1 + K_1 c_1 + K_2 c_2} N_{\text{ph}}^0(N_2) + \sum_{i=1,2} [c_i N_{\text{ph}}^0(Q_i) + c_i(1 - c_1 - c_2) N_{\text{ph}}(Q_i \rightarrow N_2)] \quad (4)$$

Table 3

The Stern–Volmer constant K in pure nitrogen. In the original model, the fit range is $c = 0–0.4$, and in the modified model, $c = 0–1$

Quencher gas	Modified Stern–Volmer (Eq. (3))			Original Stern–Volmer (Eq. (2))	
	K	$N_{\text{ph}}(Q \rightarrow N_2)$	χ^2/ν	K	χ^2/ν
O ₂	20.7 ± 1.5	7.1 ± 2.1	1.4/4	26.4 ± 1.5	1.0/3
CO ₂	45.7 ± 4.0	2.6 ± 1.7	3.7/4	48.5 ± 3.0	1.6/3
CH ₄	51.8 ± 5.1	9.3 ± 1.8	1.0/4	53.3 ± 2.7	1.8/3

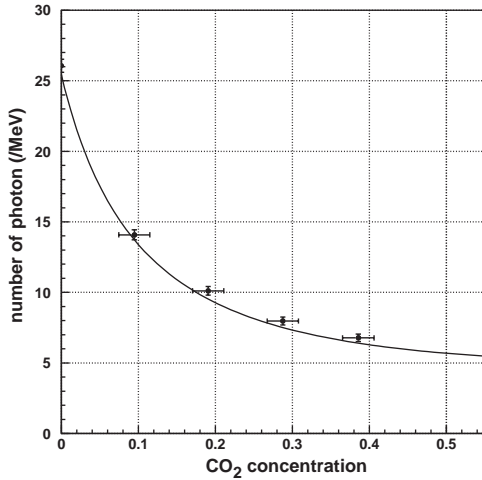


Fig. 11. CO₂ quenching effect in Air. Solid curve shows the prediction with Eq. (4).

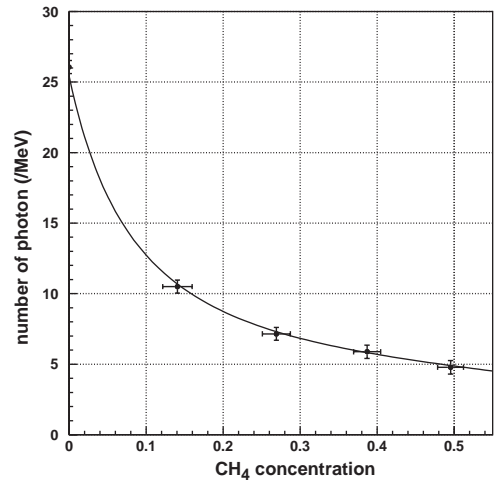


Fig. 12. CH₄ quenching effect in Air. Solid curve shows the prediction with Eq. (4).

where suffixes 1 and 2 distinguish the gas species. In the case that a quencher gas is added to the air, quenching effect is the sum of the oxygen and quencher gas, where we ignore the effect of other gas species in air. We investigate the quenching effects in air, hoping to find out appropriate gas mixture usable in the actual experiment. Figs. 11 and 12 show the measurement results obtained for the Air–CO₂ and Air–CH₄ gas mixture, respectively.

The ordinate and abscissa are the same as in Fig. 8, and the solid curves show the prediction by Eq. (4) using the measured values for the parameters $N_{\text{ph}}^0(N_2)$, $N_{\text{ph}}^0(Q_i)$, $N_{\text{ph}}(Q_i \rightarrow N_2)$ and K_i ($i = \text{O}_2, \text{CO}_2, \text{CH}_4$). The resultant values for the chi-squared per degree of freedom are $\chi^2/\nu = 4.4/5$ (CO₂) and $\chi^2/\nu = 2.3/5$ (CH₄).⁶ The agreement

⁶In evaluating χ^2/ν , we included the effects due to uncertainty in the gas mixing rate (5%) shown by the horizontal error bars.

between the prediction and the data indicates the validity of the assumption that quenching effect is additive in these gases. From Figs. 11 and 12, we conclude that we need to mix 30% of CO₂ or 20% of CH₄ to reduce the scintillation due to the air by a factor of 3.

4. Conclusions

In this paper, we have presented the measurement of the quenching effect in N₂ gas scintillation. The quenching gases studied are O₂, CO₂ and CH₄. Among these gases, CH₄ is the most effective. We find the quenching effect can be well represented by a phenomenological model of Eq. (3) for a full range of quencher gas concentration c . When two quenching gases are mixed to N₂, the effect seems to be additive. The quenching effect occurs most likely due to energy exchange by

collisions between the gas molecules. As to our original motivation of the study, we are now confident that the N₂ scintillation background can be reduced to a tolerable level by adding CO₂ or CH₄ in the air. Pure O₂ or CH₄ should be avoided for safety reasons, but CO₂ may be an option.

Acknowledgements

We thank L. Littenberg, D. Jaffe and other KOPIO collaborators for reading this paper and giving useful comments. This research was supported by the Ministry of Education, Culture, Sports, Science and Technology of Japan, under the Grant-in-Aids for Scientific Research on Priority Areas, and through the Japan-U.S. Co-operative Research Program in High Energy Physics.

Appendix A. Stern–Volmer model

A.1. Stern–Volmer model

In this appendix, we derive the Stern–Volmer model by treating quenching mechanism phenomenologically. Here, we deal with the simplest situation: one quencher gas is mixed in N₂. Let us assume, for simplicity, only one excited state of N₂ is involved in scintillation, and decays through one of four deexcitation modes: radiation (k_f), internal quenching (k_i), collisional quenching with N₂ (k_{qN_2}) or collisional quenching with quencher (k_{qQ}). The rate parameter (1/s) for each process is denoted by the quantity in the parentheses. Then, the total rate (k) can be expressed as

$$k = k_f + k_i + k_{qN_2}(1 - c) + k_{qQ}c, \quad (\text{A.1})$$

where c is the concentration of quencher gas. Note that we have neglected a scintillation term by the quencher because the actual gases we used have a very low scintillation power.

The scintillation efficiency ε can be represented by

$$\varepsilon = \frac{k_f}{k} = \frac{k_f}{k_f + k_i + k_{qN_2}(1 - c) + k_{qQ}c}. \quad (\text{A.2})$$

The number of emitted photons due to N₂ excitation is proportional to ε and the number of N₂^{*}. A straightforward calculation leads to

$$N_{\text{ph}}(N_2) = (1 - c) \frac{1}{1 + Kc} N_{\text{ph}}^0(N_2) \quad (\text{A.3})$$

where $K = (k_{qQ} - k_{qN_2}) / (k_f + k_i + k_{qN_2})$ is introduced for simplicity, and $N_{\text{ph}}^0(N_2)$ is the number of photons emitted when $c = 0$ (pure N₂).

Usually the Stern–Volmer equation is quoted as

$$N_{\text{ph}}(N_2) = \frac{N_{\text{ph}}^0(N_2)}{1 + Kc}, \quad (\text{A.4})$$

which is valid when $c \ll 1$.

A.2. Modified Stern–Volmer model

In order to make the Stern–Volmer model applicable to all range of quencher concentration c , we introduce light emission mechanism induced by quencher gas and energy transfer back to N₂^{*}. Again, we assume that one excited state of quencher gas Q^{*} deexcites through five modes: fluorescence (k'_{fQ}), internal quenching (k'_i), collision with N₂ decaying radiatively (k'_{fN_2}), or non-radiatively (k'_{qN_2}), and collisional quench with quencher gas itself (k'_{qQ}). The rate equation can be written as

$$k' = k'_{fQ} + k'_i + k'_{fN_2}(1 - c) + k'_{qN_2}(1 - c) + k'_{qQ}c \quad (\text{A.5})$$

where k' is the total rate for the excited quencher gas. We note that the term proportional to k'_{fN_2} plays an important role.⁷ The scintillation efficiency ε' for Q^{*} becomes

$$\varepsilon' = \frac{k'_{fQ} + k'_{fN_2}(1 - c)}{k'}. \quad (\text{A.6})$$

Again, a straightforward calculation leads to

$$N_{\text{ph}}(Q) = \frac{cN_{\text{ph}}^0(Q) + c(1 - c)N_{\text{ph}}(Q \rightarrow N_2)}{1 + K'(1 - c)} \quad (\text{A.7})$$

⁷It is possible to think of a situation in which k'_{fN_2} will be modified further due to tertiary processes such as collisions with other N₂ or the quencher molecules. If this is the case, k'_{fN_2} would be a function of c . However, as will be seen, the term is important only when $c \sim 0.5$; thus we have treated it as a constant for simplicity.

where $N_{\text{ph}}^0(Q)$ is the number of photons emitted when $c = 1$ (pure Q), and $K' = (k'_{\text{fN}_2} + k'_{\text{qN}_2} - k'_{\text{qQ}})/(k'_{\text{fQ}} + k'_i + k'_{\text{qQ}})$ is an equivalent of the Stern–Volmer constant K . The notation $N_{\text{ph}}(Q \rightarrow N_2)$ is introduced for convenience; it represents the number of emitted photons by the energy transfer process from Q to N_2 . We note $N_{\text{ph}}^0(Q)/N_{\text{ph}}(Q \rightarrow N_2) = k'_{\text{fq}}/k'_{\text{fN}_2}$. The total number of emitted photons is the sum of $N_{\text{ph}}(N_2)$ and $N_{\text{ph}}(Q)$:

$$N_{\text{ph}} = (1 - c) \frac{1}{1 + Kc} N_{\text{ph}}^0(N_2) + c N_{\text{ph}}^0(Q) + c(1 - c) N_{\text{ph}}(Q \rightarrow N_2). \quad (\text{A.8})$$

Here, we have neglected the $K'(1 - c)$ term in the denominator of Eq. (A.7). When $c \sim 1$, the term can be neglected while, when $c < 1$, the 1st term ($\propto N_{\text{ph}}^0(N_2)$) in Eq. (A.8) dominates the entire contribution. Thus, the term $K'(1 - c)$ is insensitive in a fitting process, and is neglected for simplicity. In addition, it is natural to expect K' not to be large ($|K'| < 1$) because the quenching term k'_i or k'_{qQ} dominates the other modes in the quenching gases we used. In summary, the 1st term in Eq. (A.8) dominates when $c < 1$ while the 2nd or 3rd term plays an important role when $c \sim 1$ or $c \sim 0.5$.

References

- [1] W. Tornow, H. Huck, H.J. Kober, G. Nertens, Nucl. Instr. and Meth. 133 (1976) 435.
- [2] M. Mutterer, J.P. Theobald, K.P. Schelhaas, Nucl. Instr. and Meth. 144 (1977) 159.
- [3] R.M. Baltrusaitis, et al., Nucl. Instr. and Meth. A 240 (1985) 410.
- [4] T. Shima, K. Watanabe, T. Irie, H. Sato, Y. Nagai, Nucl. Instr. and Meth. A 356 (1995) 347.
- [5] S.P. Garg, K.B.S. Murthy, R.C. Sharma, Nucl. Instr. and Meth. A 357 (1995) 406.
- [6] J.J. Petruzzo III, et al., Nucl. Instr. and Meth. A 402 (1998) 123.
- [7] <http://pubweb.bnl.gov/people/e926/>.
- [8] GEANT, Detector description and simulation tool, CERN Program Library Long Writeup W5013, CERN, Geneva, Switzerland, 1993.
- [9] Hamamatsu Photonics K.K., Iwata-country, Shizuoka Pref., 438-0193 Japan.
- [10] Hamamatsu Catalog, Si PIN photodiode S3590 series, Catalog No. KPIN10521.
- [11] Hamamatsu Catalog, Photomultiplier Tube R329-02, Catalog No. TPMH1254E01.
- [12] Hamamatsu Catalog, Photomultiplier Tubes and Assemblies For Scintillation Counting & High Energy Physics, Catalog No. TPMO0001E06.
- [13] M. Duquesne, I. Kaplan, J. Phys. Radium 21 (1960) 708.
- [14] J.B. Birks, The Theory and Practice of Scintillation Counting, Pergamon Press, Oxford, 1964, p. 570–614.
- [15] O. Stern, M. Volmer, Phys. Z. 20 (1919) 183.
- [16] A.E. Grun, E. Schopper, Z. Naturforsch. 6a (1951) 698.